FT-Raman, FT-IR spectra and total energy distribution of 3-pentyl-2,6-diphenylpiperidin-4-one: DFT method

S. Subashchandrabose [a], H. Saleem [a,*], Y. Erdogdu [b], G. Rajarajan [c], V. Thanikachalam [c]

[a] Department of Physics, Annamalai University, Annamalai Nagar, Tamil Nadu 608002, India
[b] Department of Physics, Ahi Evran University, Kirsehir, Turkey
[c] Department of Chemistry, Annamalai University, Annamalai Nagar, Tamil Nadu 608002, India

ABSTRACT

FT-Raman and FT-IR spectra were recorded for 3-pentyl-2,6-diphenylpiperidin-4-one (PDPO) sample in solid state. The equilibrium geometries, harmonic vibrational frequencies, infrared and the Raman scattering intensities were computed using DFT/6-31G(d,p) level. Results obtained at this level of theory were used for a detailed interpretation of the infrared and Raman spectra, based on the total energy distribution (TED) of the normal modes. Molecular parameters such as bond lengths, bond angles and dihedral angles were calculated and compared with X-ray diffraction data. This comparison was good agreement. The intra-molecular charge transfer was calculated by means of natural bond orbital analysis (NBO). Hyperconjugative interaction energy was more during the π–π^* transition. Energy gap of the molecule was found using HOMO and LUMO calculation, hence the less band gap, which seems to be more stable. Atomic charges of the carbon, nitrogen and oxygen were calculated using same level of calculation.

© 2011 Elsevier B.V. All rights reserved.

1. Introduction

Piperidones exhibit a wide spectrum of biological activities and form an essential part of the molecular structures of important drugs. Molecular geometry critically influences biological activity. Attention has been focused on structure-activity relationships. Piperidines with crowded groups at C_3 and C_5 have enhanced biological activity compared to other piperidines [1]. 2,6-Disubstituted piperidin-4-ones are regarded as an important framework and served as precursors for chiral biologically active natural alkaloids [2]. The biological activities of piperidones were found to be excellent if 2- and/or 6-positions are occupied by aryl groups [3]. Accordingly, anti-bacterial and anti-fungal activities of 2,6-diarylpiperidin-4-ones and their derivatives have been explored well [4,5]. Stereochemistry of N-benzoyl-2r,6c-diphenylpiperidin-4-one oxime, N-benzoyl-3t-methyl-2r,6c-diphenylpiperidin-4-one oxime, N-benzoyl-3t-ethyl-2r,6c-diphenylpiperidin-4-one oxime (3), N-acetyl-2r,6c-diphenylpiperidin-4-one oxime and N-acetyl-3t-methyl-2r,6c-diphenylpiperidin-4-one oxime have been studied using ^{1}H, ^{13}C and two-dimensional NMR spectra [6]. The main goal of this work is to record, simulate and interpret the vibrational spectra for the title compound, which has not been presented before. We also wanted to shed a light on the crystal and vibrational spectral data (FT-Raman and FT-IR) with the results of theoretical calculations.

2. Experimental details

2.1. Synthesis of 3-pentyl-2,6-diphenylpiperidin 4-one (PDPO) [7]

A mixture of ammonium acetate (3.85 g, 0.05 mol), benzaldehyde (10.6 ml, 0.1 mol) and 2-octanone (6.4 ml, 0.05 mol) in distilled ethanol was heated to boiling. After cooling the viscous liquid obtained was dissolved in diethyl ether (200 ml) and was shaken with 2 ml concentrated hydrochloric acid. The precipitated hydrochloride of the title compound was removed by filtration and washed with 40 ml mixture of ethanol and diethyl ether (1:1) and then with diethyl ether to remove most of the coloured impurities [7]. The base was liberated from an alcoholic solution by adding aqueous ammonia and then diluted with water. It was purified by column chromatography, using a n-hexane-ethyl acetate mixture as the solvent. The yield of the compound was 80%.

2.2. FT-Raman and FT-IR measurement

The FT-Raman spectrum of PDPO was recorded using the 1064 nm line of Nd:YAG laser as excitation wavelength in the region 10–3500 cm^{-1} on a Bruker model RFS100/S spectrophotometer

* Corresponding author. Tel.: +91 9443879295.
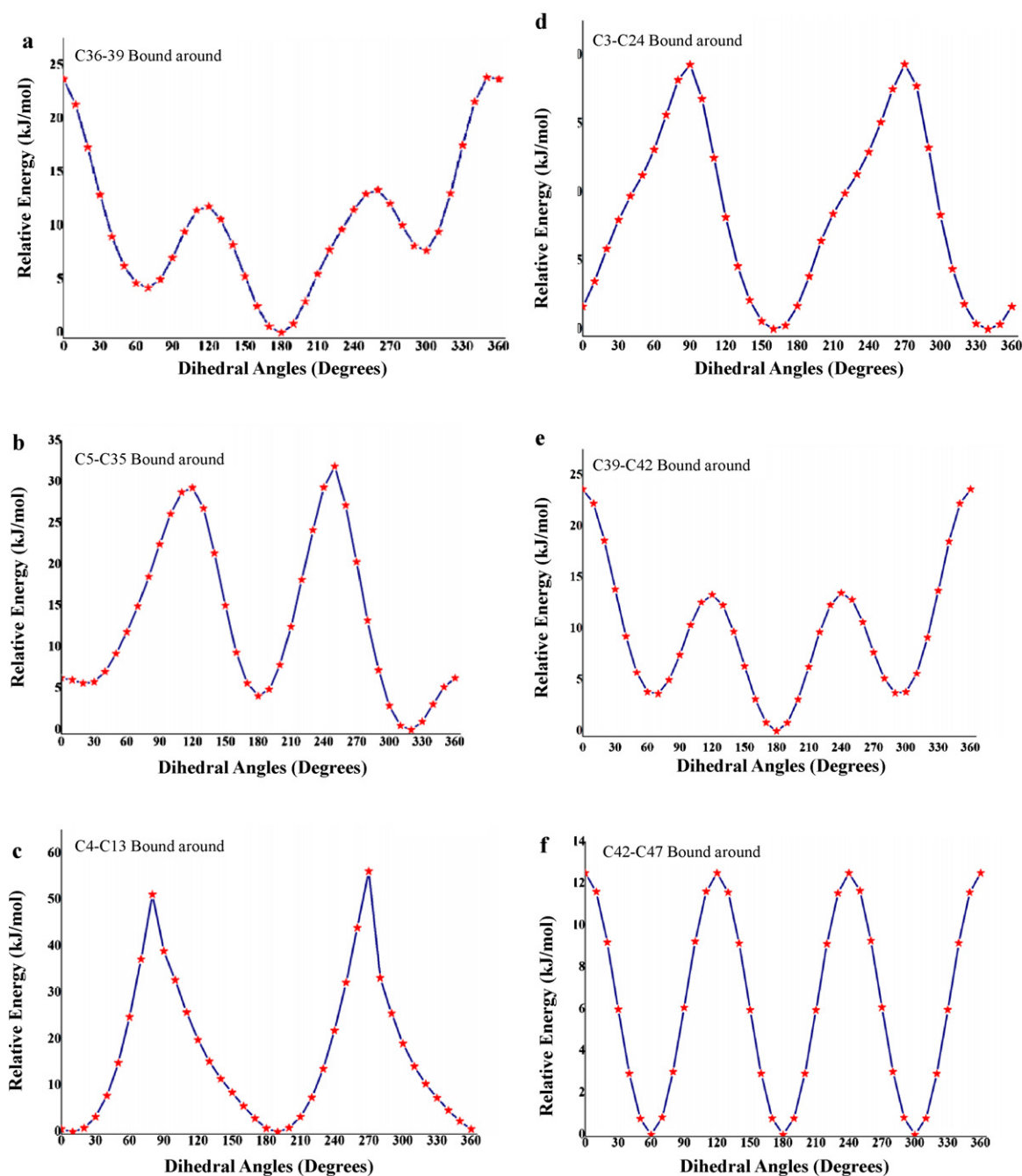E-mail address: saleem_h2001@yahoo.com (H. Saleem).

Fig. 1. (a) Relative energy–dihedral angle curve in C_{36}–C_{39} bond. (b) Relative energy–dihedral angle curve in C_5–C_{35} bond. (c) Relative energy–dihedral angle curve in C_4–C_{13} bond. (d) Relative energy–dihedral angle curve in C_3–C_{24} bond. (e) Relative energy–dihedral angle curve in C_{39}–C_{42} bond. (f) Relative energy–dihedral angle curve in C_{42}–C_{47} bond.

equipped with FRA 106 FT-Raman module accessory. The spectral measurements were carried out at Sree Chitra Tirunal Institute for Medical Sciences and Technology, Poojappura, Thiruvananthapuram, Kerala, India. The FT-IR spectrum of this compound was recorded in the region 400–4000 cm^{-1} on an IFS 66 V spectrophotometer using the KBr pellet technique. The spectrum was recorded at room temperature, with a scanning speed of 10 cm^{-1} per minute and at the spectral resolution of 2.0 cm^{-1} in CISL Laboratory, Annamalai University, Tamil Nadu, India.

3. Computational details

The entire calculations were performed at DFT levels on a Pentium 1 V/3.02 GHz personal computer using Gaussian 03W [8]

program package, invoking gradient geometry optimization [8,9]. Initial geometry generated from standard geometrical parameters was minimized without any constraint in the potential energy surface at DFT level, adopting the standard 6-31G(d,p) basis set. The optimized structural parameters were used in the vibrational frequency calculations at the DFT level to characterize all stationary points as minima. Then, vibrationaly averaged nuclear positions of PDPO were used for harmonic vibrational frequency calculations resulting in IR and Raman frequencies together with intensities and Raman depolarization ratios. In this study, the DFT method (B3LYP) was used for the computation of molecular structure, vibrational frequencies and energies of optimized structures. The vibrational modes were assigned on the basis of TED analysis using SQM program [10].
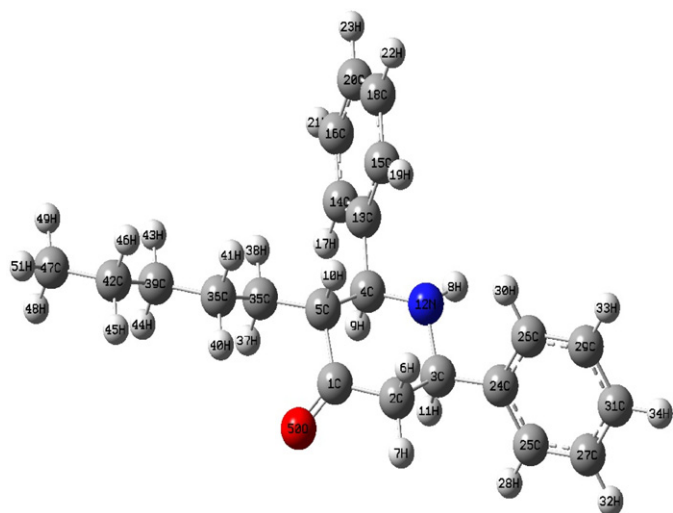
Fig. 2. Optimized molecular structure of 3-pentyl-2, 6-diphenylpiperidin-4-one.

Fig. 3. Theoretical (a) and experimental (b) FT-IR spectrum of PDPO.

It should be noted that Gaussian 03W package able to calculate the Raman activity. The Raman activities were transformed into Raman intensities using Raint program [11] by the expression:

$$I_i = 10^{-12} \frac{(\nu_0 - \nu_i)^4}{\nu_i \cdot S} \tag{1}$$

where I_i is the Raman intensity, S is the Raman scattering activities, ν_i is the wavenumber of the normal modes and ν_0 denotes the wavenumber of the excitation laser [12].

4. Results and discussion

4.1. Conformational analysis

The chair conformer of piperidine molecule is the most stable conformer. Therefore, we neglected other conformations that differ from the chair (boat, envelope or twist boat) because of their high energy. Moreover, it has two possible chair conformations, which differ in the axial (A) or equatorial (E) positions of the N–H group [13–15]. Piperidine molecules show the equatorial form of NH of chair conformer as the most stable. Piperidine molecule adopts the NH equatorial position of the chair conformer. Then, in order to reveal all possible conformations of studied molecule, a detailed potential energy surface (PES) scan in six dihedral angles was performed. This scan was carried out by relaxed PES scanning calculations in all geometrical parameters by changing the torsion angle for every 10° rotation around the bond. The shape of the potential energy as a function of the dihedral angle is illustrated in Fig. 1a–f. The curves between relative energy and dihedral angles ($a \rightarrow H_{11}$–C_3–C_{24}–C_{25} and $c \rightarrow H_9$–C_4–C_{13}–C_{14}) are shown in Fig. 1a and c. As seen in Fig. 1a and c, H_{11}–C_3–C_{24}–C_{25} dihedral angle of phenyl ring is attached with C_3 is determined at 160° for B3LYP level of theory. H_9–C_4–C_{13}–C_{14} dihedral angle is predicted at 10°. In the optimized structure, H_{11}–C_3–C_{24}–C_{25} and H_9–C_4–C_{13}–C_{14} dihedral angles are predicted at 162.24° and 9.50°, respectively.

4.2. Molecular geometry

The optimized geometrical parameters and structure of PDPO was calculated at 6-31G(d,p) level, are given in Table 1 and Fig. 2, respectively. Geometrical parameters such as bond lengths, bond angles and dihedral angles are also given along with its single crystal X-ray diffraction data. The bond length of C_1–O_{50} is about 1.218 in B3LYP method. And its corresponding experimental value
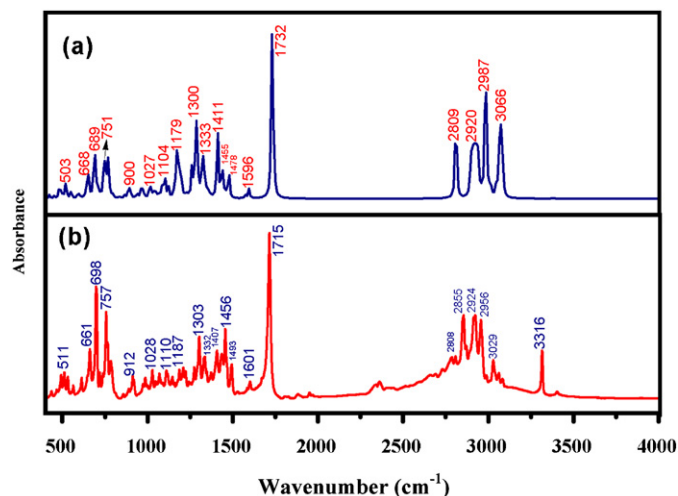
is 1.214 Å [7]. Similarly the C_3–N_{12} and C_4–N_{12} bond distances are calculated at 1.465 and 1.470 Å (DFT), which are in agreement with X-ray data. The bond distance of C–C is usually observed as ~1.400 Å. In the present investigation, bond lengths of C_1–C_2, C_1–C_5, C_2–C_3, C_3–C_{24}, C_4–C_5, C_4–C_{13} and C_5–C_{35} are in line with literature values. On the other hand, the bond distances (C_{13}–C_{14}, C_{13}–C_{15}, C_{14}–C_{16}, C_{15}–C_{18}, C_{16}–C_{20}, C_{25}–C_{27}, C_{26}–C_{29}, C_{27}–C_{31} and C_{29}–C_{31}) of the sixmembered rings are approximately 1.39 Å/B3LYP with few exceptions. These values are in agreement with literature values [7]. Crystal data [7] reveal that the C–H bond distances are ~1.00 Å, which is supported by the calculated values. The calculated angles 121.85° and 122.91° (DFT), are belongs to C_2–C_1–O_{50} and C_5–C_1–O_{50}, respectively. And their corresponding literature values are 121.93° and 122.01°. These larger bond angles are may be due to electron density in oxygen atom. The bond angle C_{14}–C_{13}–C_{15}: 118.705/B3LYP is less when comparing with other bond angles C_{13}–C_{14}–C_{16}, C_{13}–C_{15}–C_{18}, C_{14}–C_{16}–C_{20}, C_{15}–C_{18}–C_{20} and C_{16}–C_{20}–C_{18} (~120°). It may be due to the phenyl ring is attached with C_4. Similar trend has been observed in the second phenyl ring. The bond angles of C–C–H are ~109° except in both phenyl rings (~120°) which are in agreement with literature values [7]. The dihedral angles of title molecule were calculated, and some of them were compared with available X-ray diffraction data as shown in Table 1.

4.3. Vibrational assignments

Synthesized PDPO, consists 51 atoms and hence 147 normal modes of vibrations and the molecule belongs to C_1 symmetry. The fundamental vibrational wavenumbers of PDPO was calculated by DFT (B3LYP/6-31G(d,p)) is given in Table 2. The resulting vibrational wavenumbers for the optimized geometries, IR intensities as well as Raman scattering activities and experimental FT-IR, FT-Raman frequencies are also listed. Experimental and theoretical spectra of title compound have been shown in Fig. 3 (FT-IR) and Fig. 4 (FT-Raman). The normal modes of vibration were assigned on the basis of TED. To bring the theoretical values closer to experimental values, we used the scale factor: 0.9608.

4.3.1. N–H vibrations

The N–H stretching vibration [13,14] appears strongly and broadly in the region 3500–3300 cm^{-1}. Y. Erdogdu et al., assigned ν_{N-H} mode in the region 3500–3300 cm^{-1} [15]. In this study, the frequency was observed as weak and narrow band in both FT-IR and FT-Raman, where the frequencies are attributed to 3316 cm^{-1} and

Table 1
Bond lengths, bond angles and dihedral angles of PDPO.

Parameters Bond length (Å)	Exp.[a]	B3LYP/6-31G(d,p)	Parameters Angles Contd.	Exp.[a]	B3LYP/6-31G(d,p)
C_1-O_{50}	1.214	1.218	$C_5-C_1-O_{50}$	122.0	122.9
C_3-N_{12}	1.469	1.465	$C_1-C_2-H_6$	109.0	109.3
C_4-N_{12}	1.471	1.470	$C_1-C_2-H_7$	109.0	109.1
C_1-C_2	1.506	1.519	$C_3-C_2-H_6$	109.0	108.1
C_1-C_5	1.526	1.531	$C_3-C_2-H_7$	109.0	111.1
C_2-C_3	1.532	1.549	$H_6-C_2-H_7$	109.0	109.0
C_3-C_{24}	1.514	1.518	$C_2-C_3-H_{11}$	109.0	106.9
C_4-C_5	1.550	1.567	$C_2-C_3-N_{12}$	107.4	107.8
C_4-C_{13}	1.513	1.519	$H_{11}-C_3-N_{12}$	109.0	111.5
C_5-C_{35}	1.531	1.534	$H_{11}-C_3-C_{24}$	109.0	107.8
$C_{13}-C_{14}$	1.390	1.400	$N_{12}-C_3-C_{24}$	111.2	110.9
$C_{13}-C_{15}$	1.393	1.402	$C_5-C_4-H_9$	109.0	106.6
$C_{14}-C_{16}$	1.387	1.396	$C_5-C_4-N_{12}$	109.3	108.8
$C_{15}-C_{18}$	1.392	1.394	$H_9-C_4-N_{12}$	109.0	111.5
$C_{16}-C_{20}$	1.392	1.395	$H_9-C_4-C_{13}$	109.0	107.7
$C_{18}-C_{20}$	1.378	1.397	$N_{12}-C_4-C_{13}$	108.7	109.1
$C_{25}-C_{27}$	1.391	1.396	$C_1-C_5-H_{10}$	107.0	106.8
$C_{26}-C_{29}$	1.395	1.395	$C_4-C_5-H_{10}$	107.0	105.5
$C_{27}-C_{31}$	1.385	1.395	$H_{10}-C_5-C_{35}$	109.0	109.9
$C_{29}-C_{31}$	1.379	1.396	$C_3-N_{12}-C_4$	111.7	114.3
$C_{35}-C_{36}$	1.522	1.535	$C_3-N_{12}-H_8$	110.0	109.5
$C_{36}-C_{39}$	1.526	1.533	$C_4-N_{12}-H_8$	108.8	109.2
$C_{39}-C_{42}$	1.521	1.534	$C_{13}-C_{14}-H_{17}$	120.0	119.4
$C_{42}-C_{47}$	1.522	1.532	$C_{16}-C_{14}-H_{17}$	120.0	119.7
C_2-H_6	0.990	1.097	$C_{13}-C_{15}-H_{19}$	120.0	119.0
C_2-H_7	0.990	1.092	$C_{18}-C_{15}-H_{19}$	120.0	120.3
C_3-H_{11}	1.000	1.107	$C_{14}-C_{16}-H_{21}$	120.0	119.7
C_4-H_9	1.000	1.107	$C_{20}-C_{16}-H_{21}$	120.0	120.1
C_5-H_{10}	1.000	1.100	$C_{15}-C_{18}-H_{22}$	120.0	119.7
H_8-N_{12}	0.911	1.017	$C_{20}-C_{18}-H_{22}$	120.0	120.0
$C_{14}-H_{17}$	0.950	1.087	$C_{16}-C_{20}-H_{23}$	120.0	120.2
$C_{15}-H_{19}$	0.950	1.086	$C_{18}-C_{20}-H_{23}$	120.0	120.1
$C_{16}-H_{21}$	0.950	1.086	$C_{24}-C_{25}-H_{28}$	120.0	119.4
$C_{18}-H_{22}$	0.950	1.086	$C_{27}-C_{25}-H_{28}$	120.0	119.7
$C_{20}-H_{23}$	0.950	1.086	$C_{24}-C_{26}-H_{30}$	120.0	118.9
$C_{24}-C_{25}$	1.385	1.400	$C_{29}-C_{26}-H_{30}$	120.0	120.4
$C_{24}-C_{26}$	1.389	1.402	$C_{25}-C_{27}-H_{32}$	120.0	119.7
$C_{25}-H_{28}$	0.950	1.087	$C_{31}-C_{27}-H_{32}$	120.0	120.1
$C_{26}-H_{30}$	0.950	1.085	$C_{26}-C_{29}-H_{33}$	120.0	119.7
$C_{27}-H_{32}$	0.950	1.086	$C_{31}-C_{29}-H_{33}$	120.0	120.0
$C_{29}-H_{33}$	0.950	1.086	$C_{27}-C_{31}-C_{29}$	119.7	119.6
$C_{31}-H_{34}$	0.950	1.086	$C_{27}-C_{31}-H_{34}$	120.0	120.1
$C_{35}-H_{37}$	0.990	1.097	$C_{29}-C_{31}-H_{34}$	120.0	120.2
$C_{35}-H_{38}$	0.990	1.096	$C_5-C_{35}-H_{37}$	109.0	108.8
$C_{36}-H_{40}$	0.990	1.095	$C_5-C_{35}-H_{38}$	109.0	108.9
$C_{36}-H_{41}$	0.990	1.100	$C_{36}-C_{35}-H_{37}$	109.0	109.1
$C_{39}-H_{43}$	0.990	1.100	$C_{36}-C_{35}-H_{38}$	109.0	108.9
$C_{39}-H_{44}$	0.990	1.099	$H_{37}-C_{35}-H_{38}$	108.0	107.0
$C_{42}-H_{45}$	0.990	1.098	$C_{35}-C_{36}-H_{40}$	109.0	109.2
$C_{42}-H_{46}$	0.990	1.099	$C_{35}-C_{36}-H_{41}$	109.0	109.1
$C_{47}-H_{48}$	0.980	1.096	$C_{39}-C_{36}-H_{40}$	109.0	109.4
$C_{47}-H_{49}$	0.980	1.096	$C_{36}-C_{35}-H_{37}$	109.0	109.1
$C_{47}-H_{51}$	0.980	1.095	$C_{36}-C_{35}-H_{38}$	109.0	108.9
Bond angle (°)			$C_{39}-C_{36}-H_{41}$	109.0	109.0
$C_2-C_1-C_5$	116.0	115.1	$H_{40}-C_{36}-H_{41}$	108.0	106.7
$C_1-C_2-C_3$	111.4	110.0	$C_{36}-C_{39}-H_{43}$	109.0	109.4
$C_2-C_3-C_{24}$	110.8	111.7	$C_{36}-C_{39}-H_{44}$	109.0	109.2
$C_5-C_4-C_{13}$	112.3	112.8	$C_{42}-C_{39}-H_{43}$	109.0	109.2
$C_1-C_5-C_4$	109.6	107.6	$C_{42}-C_{39}-H_{44}$	109.0	109.1
$C_1-C_5-C_{35}$	107.0	112.4	$H_{43}-C_{39}-H_{44}$	108.0	106.0
$C_4-C_5-C_{35}$	112.1	113.9	$C_{39}-C_{42}-H_{45}$	109.0	109.1
$C_4-C_{13}-C_{14}$	120.9	120.7	$C_{39}-C_{42}-H_{46}$	109.0	109.2
$C_4-C_{13}-C_{15}$	120.4	120.5	$H_{45}-C_{42}-H_{46}$	108.0	105.9
$C_{14}-C_{13}-C_{15}$	109.0	118.7	$H_{45}-C_{42}-C_{47}$	109.0	109.4
$C_{13}-C_{14}-C_{16}$	120.9	120.8	$H_{46}-C_{42}-C_{47}$	109.0	109.4
$C_{13}-C_{15}-C_{18}$	120.8	120.6	$C_{42}-C_{47}-H_{48}$	109.0	111.1
$C_{14}-C_{16}-C_{20}$	119.6	120.0	$C_{42}-C_{47}-H_{49}$	109.0	111.2
$C_{15}-C_{18}-C_{20}$	120.3	120.2	$C_{42}-C_{47}-H_{51}$	109.0	111.5
$C_{16}-C_{20}-C_{18}$	119.9	119.6	$H_{48}-C_{47}-H_{49}$	109.0	107.4
$C_3-C_{24}-C_{25}$	119.9	120.2	$H_{48}-C_{47}-H_{51}$	109.0	107.6
$C_3-C_{24}-C_{26}$	121.1	120.9	$H_{49}-C_{47}-H_{51}$	109.0	107.6
$C_{25}-C_{24}-C_{26}$	118.8	118.8	Dihedral (°)		
$C_{24}-C_{25}-C_{27}$	120.3	120.7	$C_2-C_3-N_{12}-C_4$	−66.82	−62.88
$C_{24}-C_{26}-C_{29}$	120.8	120.5	$C_{24}-C_3-N_{12}-C_4$	172.32	174.49

Table 1 (*Continued*)

| Parameters Bond length (Å)	Exp.[a]	B3LYP/6-31G(d,p)	Parameters Angles Contd.	Exp.[a]	B3LYP/6-31G(d,p)
C_{25}–C_{27}–C_{31}	120.8	120.0	N_{12}–C_4–C_5–C_1	−51.99	−54.54
C_{26}–C_{29}–C_{31}	120.7	120.2	N_{12}–C_4–C_5–C_{35}	−178.04	−179.93
C_5–C_{35}–C_{36}	113.4	113.6	C_{13}–C_4–C_5–C_1	−172.73	−175.84
C_{35}–C_{36}–C_{39}	113.7	112.9	C_{13}–C_4–C_5–C_{35}	61.21	58.77
C_{36}–C_{39}–C_{42}	112.8	113.4	C_{13}–C_4–N_{12}–C_3	−171.28	−172.35
C_{39}–C_{42}–C_{47}	113.7	113.2			
C_2–C_1–O_{50}	121.9	121.8			
C_2–C_1–O_{50}	122.0	122.9			

[a] Ref. [7].
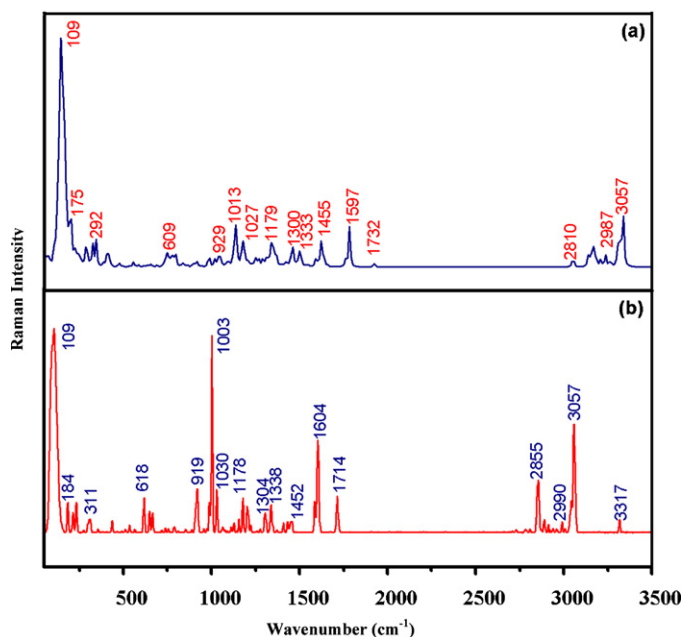
Fig. 4. Theoretical (a) and experimental (b) FT-Raman spectrum of PDPO.

3317 cm^{-1} respectively. The corresponding theoretical frequency for $\nu_{\text{N–H}}$ mode is about 3384 cm^{-1}, which shows positive deviation of ~68 cm^{-1} from the experimental value. The scissoring mode of N–C–H is appeared at 1407 cm^{-1} (FT-IR-strong) and 1409 cm^{-1} (FT-Raman-weak), while the harmonic scissoring vibration existed at 1411 cm^{-1} (mode no. 104). These $\delta_{\text{C–N–H}}$ wavenumbers are also find support from the literature. Out-of-plane bending modes ($\gamma_{\text{C–N–H}}$) are calculated at about 765 and 771 cm^{-1} (mode nos. 44, 45), these vibrations are in line with the observed FT-IR (765 cm^{-1}) and FT-Raman (785 cm^{-1}) bands.

4.3.2. Methyl and methylene group vibrations

Methyl groups are generally referred to as electron donating substituents in the aromatic ring system [16]. In acetates, the asymmetric vibrations of the methyl group are expected to occur in the region $2940–3040 \text{ cm}^{-1}$ and symmetric vibrations are in the region $2910–2930 \text{ cm}^{-1}$, and usually the bands are weak [17]. Aromatic acetyl substituents absorb in a narrow range $3000–3020 \text{ cm}^{-1}$ absorption sometimes coincides with a CH stretching mode of the ring [17]. The title molecule possesses methyl (CH_3) and methylene (CH_2) groups. Methyl group symmetric stretching vibrations are appeared at 2914 cm^{-1} as a strong intense band in FT-IR and 2913 cm^{-1} as a very weak band in FT-Raman spectrum. While the scaled harmonic frequency 2917 cm^{-1} (mode no: 127) with considerable intensity is in line with experimental value. The asymmetric of CH_3 harmonic frequency 2987 cm^{-1} (mode no: 135) is

coincide well with experimental values (FT-IR: 2989/FT-Raman: 2990 cm^{-1}).

The asymmetric and symmetric CH_2 stretching vibrations are normally appear in the region $3100–2900 \text{ cm}^{-1}$ [18]. According to the literature [18], the observed bands 2870 cm^{-1} (weak), 2924 cm^{-1} (strong) in FT-IR and 2890 cm^{-1} (weak) FT-Raman are in agreement with the theoretical values in the range of $2891–2937 \text{ cm}^{-1}$ (mode nos: 123–126, 128–130). The FT-IR band 2956 cm^{-1} (strong) and its corresponding theoretical value 2960 cm^{-1} (mode no: 132) are attributed ν_{asy} CH_2 vibration. The TED value shows that these vibrations are pure. In aromatic compounds the $\nu_{\text{C–H}}$, $\beta_{\text{C–H}}$ and $\gamma_{\text{C–H}}$ modes are appeared in the range of $3000–3100 \text{ cm}^{-1}$, $1000–1300$ and $750–1000 \text{ cm}^{-1}$, respectively [19–21]. The C–H stretching vibrations appeared at 2810, $3048–3077 \text{ cm}^{-1}$ (mode nos: 122, 137–144). The observed frequencies 2855, 3061 cm^{-1} (FT-IR) and 2856, 3042, 3057 cm^{-1} (FT-Raman) are belongs to C–H stretching mode. The C–H in-plane bending vibrations appeared in the range $1123–1170 \text{ cm}^{-1}$ (mode nos: 76, 79, 81) and their corresponding experimental wavenumbers 1118, 1145, 1155 (FT-IR) and 1129, 1156 cm^{-1} (FT-Raman) are in consistent with computed values. The assignments also find support from the literature [22,23].

The scissoring mode of the CH_2 group gives rise to a characteristic band near 1415 cm^{-1} in IR and 1400 cm^{-1} in Raman spectra. The twisting, wagging and rocking vibrations appear in the region $1400–900 \text{ cm}^{-1}$ [24]. The broadening and intensity decreases were observed for the bands at 1470 and 1450 cm^{-1} corresponding to CH_2 scissoring modes [22]. In the present investigation, δ_{CH2} mode appear at 1436 and 1456 cm^{-1} as medium band at FT-IR, and their FT-Raman counter parts are 1452 and 1432 cm^{-1} as weak bands. These experimental frequencies are in agreement with mode nos: 106 and 111 of B3LYP. A major coincidence of theoretical values with that of experimental observation is found for ω_{CH2} (1348:B3LYP-mode no: 100/1347 cm^{-1}: FT-IR). These assignments find support from the literature [22]. In the case of CH_2 twisting mode the vibrational frequencies observed at 1274, 1303 cm^{-1} (FT-IR) and 1304 cm^{-1} (Raman) are in agreement with the calculated frequencies in the range of $1278–1300 \text{ cm}^{-1}$ (mode no: 90, 92–94/DFT). The out-of-plane bending mode of C–H always lies in the lower side of spectra. In the present study, the harmonic wavenumbers (mode nos: 60–58, 56, 54–52, 48, 47, 43–40) in the range of $962–706 \text{ cm}^{-1}$ are assigned to $\gamma_{\text{C–H}}$ mode, which find support from the observed FT-IR frequencies: 912, 889, 757 and 738 cm^{-1}.

4.3.3. C=O, C–N, C=C vibrations

Stretching vibration of carbonyl group C=O can be observed as a very strong band in both FT-IR and FT-Raman spectra at 1665 cm^{-1} [22]. The carbonyl stretching C=O vibration [17,25] is expected to occur in the region $1715–1680 \text{ cm}^{-1}$. The deviation of the calculated wavenumbers for this mode can be attributed to the underestimation of the large degree of π-electron delocalization due to conjugation of the molecule [26]. The literature

Table 2
Vibrational wave numbers obtained for PDPO at B3LYP/6-31G(d,p).

Mode no.	Computed values		Experimental		Intensity		TED[d] ($\geq$10%)
	Unscaled	Scaled[a]	FT-IR	FT-Raman	I_{IR}[b]	I_{Raman}[c]	
1	22	21			0.06	77.4	Γ_{CCCC} (40)
2	27	26			0.09	34.2	$\Gamma_{C35C5C1C2}$ (12), $\Gamma_{C35C5C1O50}$ (12)
3	30	29			0.10	68.7	$\Gamma_{C25C24C3N12}$ (16), $\Gamma_{C26C24C3N12}$ (13)
4	40	38			0.04	100	$\Gamma_{C14C13C4N12}$ (24), $\Gamma_{C14C13C4C5}$ (21), $\Gamma_{C15C13C4N12}$ (16)
5	49	47			0.04	2.04	Γ_{CCCC} (20), Γ_{HCCC} (12)
6	49	47			0.00	59.9	δ_{NCC} (12)
7	77	74			0.71	7.40	Γ_{CCCC} (13), Γ_{CCCO} (13)
8	80	77			0.01	1.44	δ_{CCC} (18), Γ_{CCCC} (16)
9	90	86			0.10	9.80	δ_{CCC} (19), Γ_{CCCC} (15)
10	113	109		109vs	0.63	4.16	Γ_{CCCO} (14)
11	127	122			0.19	2.84	$\Gamma_{C47C42C39C36}$ (12)
12	140	135			0.11	1.35	Γ_{CCCC} (14)
13	174	167			0.32	7.57	δ_{CCC} (26), ν_{CC} (16)
14	182	175		184w	0.45	1.05	$\delta_{C26C24C3}$ (12)
15	209	201			0.25	6.28	δ_{CCC} (15), ν_{CC} (14)
16	230	221		215w	0.24	7.64	Γ_{CCCC} (18)
17	250	240		233w	0.00	0.01	$\Gamma_{H51C47C42C39}$ (21), $\Gamma_{H48C47C42C39}$ (19), $\Gamma_{H49C47C42C39}$ (19)
18	269	258			0.29	1.07	δ_{CCC} (24)
19	289	277			0.24	2.54	δ_{CCC} (15)
20	297	285			2.35	2.94	δ_{CCC} (19)
21	304	292		311w	0.46	2.21	$\delta_{C25C24C3}$ (12), $\delta_{C26C24C3}$ (11)
22	358	344			1.73	1.24	ν_{CC} (24)
23	378	363			0.16	0.38	$\delta_{C39C36C35}$ (13), $\delta_{C47C42C39}$ (13)
24	417	401			0.09	0.07	$\Gamma_{C20C16C14C13}$ (14), $\Gamma_{C20C18C15C13}$ (13)
25	418	401			0.08	0.19	$\Gamma_{C31C27C25C24}$ (14), $\Gamma_{C31C29C26C24}$ (13)
26	441	424	436w	347w	1.48	1.64	δ_{CCC} (26)
27	469	451	466w		0.92	0.66	$\delta_{C42C39C36}$ (14)
28	505	485	492ms		6.99	0.57	$\delta_{C2C1O50}$ (10)
29	524	503	511w		1.61	0.63	Γ_{CCCC} (10)
30	541	520	531m	536w	6.46	0.80	δ_{NCC} (10)
31	573	551	553w		3.67	0.58	δ_{CCN} (10)
32	613	589			1.01	0.52	δ_{NCC} (10)
33	623	599			1.96	2.30	δ_{CCC} (21)
34	634	609			0.02	2.28	$\delta_{C20C16C14}$ (15), $\delta_{C20C18C15}$ (15)
35	634	609	612w	618m	0.03	3.13	$\delta_{C31C29C26}$ (16), $\delta_{C27C25C24}$ (14)
36	656	630			0.75	4.40	ν_{CC} (13), δ_{CCC} (10)
37	676	649		648w	16.1	5.74	ν_{CC} (10), δ_{CCC} (10), Γ_{HNCC} (10)
38	716	688	661s	665w	15.2	0.73	$\Gamma_{H23C20C16C14}$ (11), $\Gamma_{H23C20C18C15}$ (11)
39	717	689	698s		11.8	0.61	$\Gamma_{H34C31C27C25}$ (10), $\Gamma_{H34C31C29C26}$ (10)
40	734	706			6.29	0.56	Γ_{HCCH} (40)
41	748	719			0.91	0.46	ν_{CC} (10), Γ_{HCCC} (10)
42	775	744	738s		16.6	0.51	Γ_{HCCC} (26)
43	781	751	757s		7.40	0.57	Γ_{HCCC} (25)
44	796	765	765s		17.1	1.65	ν_{C5C1} (13), Γ_{HNCC} (10)
45	802	771	784s		6.96	0.51	Γ_{HNCC} (10)
46	826	794			1.86	0.33	ν_{C13C4} (12)
47	863	829			0.07	1.06	Γ_{HCCC} (46)
48	867	833			0.14	2.23	Γ_{HCCC} (58)
49	870	836			0.33	0.42	ν_{CC} (10)
50	900	864	857w		1.20	2.08	ν_{C42C39} (25), $\delta_{H51C47C42}$ (17), ν_{C47C42} (13)
51	917	881			0.75	2.04	ν_{C3C2} (24), δ_{N12C3} (10), δ_{C3C2H} (10)
52	926	890	889w		4.38	2.99	ν_{CC} (20), Γ_{HCCH} (10)
53	932	896			1.19	0.85	$\Gamma_{H32C27C25H28}$ (10)
54	936	900	912w		1.97	0.61	Γ_{HCCC} (10)
55	967	929		919m	0.84	1.30	ν_{C3C2} (14), δ_{CCCH} (10)
56	976	938			0.06	0.07	$\Gamma_{H22C18C15H19}$ (20), $\Gamma_{H21C16C14H17}$ (19)
57	980	941			0.94	0.65	ν_{C5C4} (14), ν_{C36C35} (14)
58	980	942			0.51	0.37	$\Gamma_{H32C27C25H28}$ (15), $\Gamma_{H33C29C26H30}$ (13)
59	1000	961			0.24	0.03	$\Gamma_{H23C20C18H22}$ (23), $\Gamma_{H23C20C16H21}$ (20), $\Gamma_{H22C18C15H19}$ (15)
60	1002	962			1.05	0.32	$\Gamma_{H34C31C29H33}$ (21), $\Gamma_{H33C29C26H30}$ (17), $\Gamma_{H34C31C27H32}$ (16)
61	1005	966			6.19	2.52	ν_{CC} (10)
62	1017	977	973w		0.70	3.29	δ_{CCC} (28), ν_{CC} (16)
63	1017	977			0.50	12.5	δ_{CCC} (40)
64	1033	992	986w	988m	0.43	0.64	ν_{C47C42} (39), ν_{C39C36} (23)
65	1054	1013	1001w	1003vs	1.74	3.13	ν_{C36C35} (17), ν_{C20C16} (12), ν_{C20C18} (10)
66	1055	1014			4.86	2.07	ν_{C31C27} (19), ν_{C31C29} (18)
67	1059	1018			1.18	4.34	ν_{C36C35} (25)
68	1069	1027	1028w	1030m	0.33	2.71	ν_{C42C39} (29), ν_{C39C36} (24), ν_{C47C42} (21)
69	1077	1035			3.12	1.23	ν_{C35C5} (29)
70	1091	1049	1046w		2.16	1.23	ν_{N12C4} (18)
71	1104	1061	1056w		1.01	0.29	δ_{CCH} (18), ν_{CC} (9), ν_{NC} (10)

Table 2 (*Continued*)

Mode no.	Computed values		Experimental		Intensity		TED[d] (≥10%)
	Unscaled	Scaled[a]	FT-IR	FT-Raman	I_{IR}[b]	I_{Raman}[c]	
72	1115	1071	1068w		1.77	0.67	ν_{N12C4} (11)
73	1130	1086	1086w		4.26	2.22	ν_{C3C2} (12), ν_{N12C3} (12)
74	1144	1099			6.61	1.31	ν_{CC} (16), δ_{CCC} (11), ν_{NC} (10)
75	1149	1104	1110m		5.33	1.44	ν_{N12C3} (23)
76	1169	1123			4.60	1.99	δ_{HCC} (13), ν_{NC} (11)
77	1187	1140	1118w	1129w	0.02	1.30	$\delta_{H34C31C27}$ (17), $\delta_{H34C31C29}$ (17)
78	1187	1141	1145w		0.06	1.32	$\delta_{H23C20C16}$ (17), $\delta_{H23C20C18}$ (16)
79	1204	1156	1155w	1156w	1.26	1.45	δ_{CCH} (22), ν_{CC} (10)
80	1205	1158			0.46	1.56	ν_{CC} (12)
81	1217	1170			20.8	1.46	ν_{CC} (13), δ_{HCC} (10)
82	1222	1174			0.06	5.22	ν_{C13C4} (26)
83	1227	1179	1187m	1178m	13.5	4.08	ν_{C24C3} (17)
84	1242	1193			5.13	0.82	δ_{CCH} (10), δ_{HCC} (11)
85	1246	1197	1209m	1203m	9.57	4.59	δ_{HCC} (13), ν_{CC} (10)
86	1274	1224	1222w		1.31	0.65	δ_{CCH} (13)
87	1283	1233			0.95	0.30	δ_{HCC} (20)
88	1298	1247	1241w		0.21	1.15	δ_{CCH} (10)
89	1313	1261	1253w		16.7	1.08	ν_{CC} (14)
90	1330	1278	1274w		2.41	0.68	ν_{CC} (14), δ_{HCH} (11)
91	1335	1283			13.4	0.69	ν_{CC} (12)
92	1338	1285			10.0	4.76	$\delta_{C42C39H44}$ (11)
93	1342	1289			21.3	1.53	δ_{CCH} (18), δ_{HCC} (17)
94	1353	1300	1303s	1304m	1.60	0.69	$\delta_{C36C35H38}$ (10)
95	1361	1308			0.51	0.19	ν_{C29C26} (10)
96	1361	1308			0.91	0.19	ν_{C18C15} (10)
97	1372	1319			7.13	1.06	δ_{HCC} (21)
98	1380	1326	1332m		12.9	3.70	$\delta_{H11C3C2}$ (10)
99	1387	1333	1336m	1338m	8.32	1.63	δ_{CCH} (13)
100	1403	1348	1347w		2.85	0.08	δ_{CCH} (10), δ_{HCC} (15)
101	1414	1358			2.41	0.21	δ_{HCN} (12)
102	1416	1360			0.49	0.42	ν_{CC} (10), δ_{HCC} (12), δ_{CCC} (15)
103	1427	1371	1372w		0.57	0.54	$\delta_{H48C47H51}$ (17), $\delta_{H48C47C42}$ (15), $\delta_{H48C47H49}$ (15)
104	1468	1411	1407m	1409w	30.5	0.94	$\delta_{C3N12H8}$ (21), $\delta_{C4N12H8}$ (21)
105	1475	1417			2.20	2.41	δ_{H6C2H7} (28)
106	1493	1434	1436m	1432w	2.95	0.68	$\delta_{H37C35H38}$ (23)
107	1497	1439			7.59	0.22	$\delta_{H34C31C27}$ (12), $\delta_{H34C31C29}$ (11)
108	1498	1439			4.66	0.33	$\delta_{H23C20C16}$ (11), $\delta_{H23C20C18}$ (10)
109	1500	1442			0.08	5.92	$\delta_{H43C39H44}$ (16)
110	1504	1445			0.27	1.02	$\delta_{H45C42H46}$ (13)
111	1514	1455	1456s	1452w	2.70	2.91	$\delta_{H48C47H51}$ (28), $\delta_{H49C47H51}$ (23)
112	1517	1458			0.10	1.13	$\delta_{H48C47H49}$ (15), $\delta_{H40C36H41}$ (11)
113	1527	1467			1.58	0.19	$\delta_{H48C47H49}$ (11)
114	1538	1477			7.05	0.03	ν_{CC} (23)
115	1538	1478	1493m		4.49	0.30	ν_{CC} (23)
116	1641	1576	1559w		0.15	0.75	ν_{C20C16} (13), ν_{C20C18} (11)
117	1642	1577	1585w	1586m	1.09	1.24	ν_{C31C27} (13), ν_{C26C24} (10), υ_{C31C29} (11)
118	1661	1596	1601w		1.89	5.28	ν_{C16C14} (20), ν_{C18C15} (20)
119	1662	1597	1654w	1604s	2.46	7.59	ν_{C27C25} (20), ν_{C29C26} (20)
120	1803	1732	1715vs	1714m	100	1.41	ν_{O50C1} (90)
121	2923	2809	2808m		6.00	0.17	ν_{C4H9} (71), ν_{C3H11} (29)
122	2925	2810	2855s	2856m	40.8	3.01	ν_{C3H11} (71), ν_{C4H9} (29)
123	3009	2891	2870w	2890w	3.21	2.85	ν_{C39H43} (46), ν_{C39H44} (38), ν_{C36H41} (10)
124	3014	2896			3.82	0.34	ν_{C36H41} (70)
125	3024	2905			13.3	0.88	ν_{C42H46} (44), ν_{C42H45} (24), ν_{C5H10} (21)
126	3025	2907			15.2	2.36	ν_{C5H10} (72), ν_{C42H46} (10)
127	3036	2917	2914s	2913w	19.5	3.90	ν_{C47H49} (37), ν_{C47H48} (33), ν_{C47H51} (26)
128	3039	2920	2924s		3.68	2.61	ν_{C39H44} (42), ν_{C39H43} (19), ν_{C42H45} (23)
129	3049	2929			16.2	1.72	ν_{C35H37} (51), ν_{C35H38} (41)
130	3057	2937			5.29	1.45	ν_{C2H6} (82), ν_{C2H7} (16)
131	3061	2941			14.9	0.24	ν_{C42H45} (32), ν_{C42H46} (26), ν_{C39H44} (15)
132	3081	2960	2956s		1.75	2.04	ν_{C36H40} (46) ν_{C35H38} (23), $\nu_{C35\ H37}$ (20)
133	3101	2979			9.65	0.06	ν_{C35H38} (32), ν_{C36H40} (31), $\nu_{C35\ H37}$ (20)
134	3105	2983			44.3	0.89	ν_{C47H49} (43), ν_{C47H48} (38)
135	3109	2987	2989w	2990w	22.9	3.03	ν_{C47H51} (72), ν_{C47H48} (17), ν_{C47H49} (10)
136	3135	3012	3029m		6.52	2.04	ν_{C2H7} (83), ν_{C2H6} (17)
137	3172	3048		3042w	3.11	0.76	ν_{C25H28} (68), ν_{C27H32} (22)
138	3174	3049			2.88	0.62	ν_{C14H17} (62), ν_{C16H21} (24)
139	3181	3056			0.18	2.37	ν_{C29H33} (46), ν_{C31H34} (31), ν_{C25H28} (17)
140	3181	3057		3057s	0.13	2.88	ν_{C18H22} (47), ν_{C20H23} (26), ν_{C14H17} (19)
141	3191	3066	3061m		9.09	3.01	ν_{C27H32} (37), ν_{C29H33} (28), ν_{C31H34} (15), ν_{C25H28} (11)
142	3192	3067			13.6	2.21	ν_{C16H21} (35), ν_{C18H22} (23), ν_{C20H23} (18), ν_{C14H17} (13)
143	3202	3077			20.4	1.22	ν_{C15H19} (33), ν_{C16H21} (25), ν_{C20H23} (23)

Table 2 (*Continued*)

Mode no.	Computed values		Experimental		Intensity		TED[d] ($\geq$10%)
	Unscaled	Scaled[a]	FT-IR	FT-Raman	I_{IR}[b]	I_{Raman}[c]	
144	3203	3077			10.1	3.64	ν_{C27H32} (28), ν_{C31H34} (28), ν_{C26H30} (25)
145	3209	3083			4.40	4.52	ν_{C15H19} (41), ν_{C18H22} (23), ν_{C20H23} (20)
146	3210	3084	3084m		6.31	8.84	ν_{C26H30} (53), ν_{C29H33} (21), ν_{C3H34} (13)
147	3522	3384	3316s	3317w	0.16	1.76	ν_{N12H8} (100)

ν: stretching, δ: bending, T: torsion, vw: very week, w: week, m: medium, s: strong, vs: very strong.

[a] Scaling factor: 0.9608 [28].
[b] Relative absorption intensities normalized with highest peak absorption equal to 100.
[c] Relative Raman intensities calculated by Eq. (1) and normalized to 100.
[d] Total energy distribution calculated B3LYP 6-31G(d,p) level, TED less than 10% are not shown.

Table 3
Second order perturbation theory analysis of Fock matrix in NBO basis (PDPO).

Donor (i)	ED/e	Acceptor (j)	ED/e	$E^{(2)}$ (kJ/mol)[a]	$E(j) - E(i)$ a.u.[b]	$F(i, j)$ (a.u.)[c]
π $C_{13}-C_{15}$	1.656	π^* $C_{14}-C_{16}$	0.335	19.77	0.28	0.066
		π^* $C_{18}-C_{20}$	0.332	20.59	0.28	0.068
π $C_{14}-C_{16}$	1.669	π^* $C_{13}-C_{15}$	0.342	20.99	0.28	0.069
		π^* $C_{18}-C_{20}$	0.332	19.69	0.28	0.066
π $C_{18}-C_{20}$	1.664	π^* $C_{13}-C_{15}$	0.342	19.50	0.28	0.066
		π^* $_{14}-C_{16}$	0.335	20.74	0.28	0.068
π $C_{24}-C_{25}$	1.659	π^* $C_{26}-C_{29}$	0.327	19.32	0.28	0.066
		π^* $C_{27}-C_{31}$	0.330	20.60	0.28	0.068
π $C_{26}-C_{29}$	1.663	π^* $C_{24}-C_{25}$	0.347	21.53	0.28	0.070
		π^* $C_{27}-C_{31}$	0.330	19.92	0.28	0.067
π $C_{27}-C_{31}$	1.662	π^* $C_{24}-C_{25}$	0.375	19.42	0.28	0.066
		π^* $C_{26}-C_{29}$	0.327	20.41	0.28	0.067
σC_3-N_{12}	1.979	σ^* C_3-C_{24}	0.029	0.57	1.09	0.022
		σ^* C_4-N_{12}	0.022	0.56	1.04	0.022
		σ^* C_4-C_{13}	0.030	2.2	1.09	0.044
σC_4-N_{12}	1.981	σ^* C_3-N_{12}	0.022	0.53	1.04	0.021
		σ^* C_3-C_{24}	0.029	2.19	1.09	0.044
		σ^* C_4-C_{13}	0.030	0.55	1.09	0.022
		C_2-C_3	0.024	1.46	0.67	0.028
		C_3-H_{11}	0.032	5.81	0.79	0.061
LPN_{12}	1.927	C_4-C_5	0.033	1.49	0.68	0.029
		C_4-H_9	0.039	5.81	0.79	0.061
		$C_{15}-H_{19}$	0.014	0.54	0.82	0.019
		C_1-C_2	0.052	0.88	1.07	0.028
LPO50 (1)	1.971	C_1-C_5	0.063	2.56	1.07	0.047
		$C_{36}-H_{40}$	0.027	4.55	1.25	0.067
		C_1-C_2	0.052	17.62	0.64	0.096
		C_1-C_5	0.063	15.93	0.62	0.016
LPO(2)	1.897	C_2-C_3	0.024	0.51	0.62	0.016
		$C_{36}-C_{39}$	0.032	0.55	0.68	0.018
		$C_{36}-H_{40}$	0.027	5.32	0.82	0.060

[a] $E^{(2)}$ means energy of hyperconjucative interactions (stabilization energy).
[b] Energy difference between donor and acceptor i and j NBO orbitals.
[c] $F(i, j)$ is the Fock matrix element between i and j NBO orbitals.

[27] reveals that the normal esters are characterized by the strong IR absorption due to the C=O stretching vibration in the range of 1750–1735 cm^{-1}. In this study, we have observed stretching of C=O at 1715 cm^{-1} as very strong in FT-IR and 1714 cm^{-1} as medium intense band in FT-Raman, while the computed frequency is 1732 cm^{-1} (mode no: 120) and its TED value (90%). The C–C stretching in phenyl ring and methylene chain is calculated in the range of 1035–864 cm^{-1} (mode nos: 69–64, 62, 61, 57, 55, and 52–50). These vibrations are in line with experimental values (1028, 1001, 986, 973, 889, 857: FT-IR and 1030, 1003, 988, 919 cm^{-1}: FT-Raman) and also in consistent with literature values [22,23]. These assignments are further supported by the TED values.

The identification of C–N vibration is a very difficult task, since mixing of several bands are possible in this region. However, with the help of theoretical calculation (DFT), the C–N stretching vibrations are calculated. The C–N stretching vibration coupled with scissoring of N–H, is moderately to strongly active in the region 1275 ± 55 cm^{-1} [17]. In the present investigation C–N

stretching frequencies are observed at 1046, 1056, 1068,1086 and 1110 cm^{-1} by FT-IR and their corresponding calculated wavenumbers appeared in the range of 1049–1104 cm^{-1} (mode nos: 70–76). These experimental values of C–N stretching mode show good agreement with theoretical values. The νC–N stretching vibration normally appears around 1300 cm^{-1} [17]. In this work the νC–N frequencies are moderately lowered, which may be due to the mass effect around nitrogen atom.

5. NBO analysis

The hyperconjugation may be given as stabilizing effect that arises from an overlap between an occupied orbital with another neighboring electron deficient orbital when these orbitals are properly orientation. This non-covalent bonding–antibonding interaction can be quantitatively described in terms of the NBO analysis, which is expressed by means of the second-order

perturbation interaction energy ($E^{(2)}$) [29–32]. This energy represents the estimation of the off-diagonal NBO Fock matrix elements. It can be deduced from the second-order perturbation approach [33]

$$E^{(2)} = \Delta E_{ij} = q_i \frac{F(i,j)^2}{\varepsilon_j - \varepsilon_i} \qquad (2)$$

where q_i is the donor orbital occupancy, ε_i and ε_j are diagonal elements (orbital energies) and $F(i,j)$ is off diagonal NBO Fock matrix elements. In this present study we dealt with NBO analysis. Especially the amount of energy transfer from π bond orbital to anti bond π^* orbital, the stabilization energy $E^{(2)}$ associated with hyperconjugative interaction, LPO(2) → C_1–C_2, and C_1–C_5 are obtained as 17.62 and 15.93 kJ/mol, respectively. The bond C_{13}–C_{15} with electron density 1.656e, stabilize the energy of 19.77 and 20.59 kJ/mol to its acceptor anti bonding orbitals of C_{14}–C_{16} and C_{18}–C_{20}, respectively. These interactions are observed as an increase in electron density (ED) in C–C antibonding orbital that weaken their bonds [34]. This investigation clearly demonstrates that the occupancy value of bonding orbitals make sure the hyperconjugative interaction with maximum stabilization between filled and unfilled subsystem of the molecule. The ED of C_{14}–C_{16} donor bond has ~1.669e, on the other hand its antibond ED (π^* C_{13}–C_{15} and C_{18}–C_{20}) posses ~0.342 and 0.332e, and their $E^{(2)}$ energies are 20.99 and 19.69 kJ/mol respectively. From the NBO analysis, the lower the ED of donor with larger the ED of acceptor have maximum delocalization and become strong bond interaction. The higher the ED value with lower $E^{(2)}$ energy which becomes lesser interaction and hence it shifts the vibrational frequencies from the actual frequencies. It is evident that the C_3–N_{12} (1.979e) and C_4–N_{12} (1.981e) bond stretching vibration (in the range from 1049 to 1123; mode nos. 70–76) lowers from the normal C–N bond stretching (1300 cm^{-1}) [17]. This may be due to the lesser hyperconjugative interaction between C–N donor bonds to C–C acceptor bands. The $E^{(2)}$ values and types of the transition are shown in Table 3.

6. HOMO–LUMO

The frontier molecular orbitals play an important role in the electric and optical properties, as well as in UV–vis spectra and chemical reactions [35]. The analysis of the wave function indicates that the electron absorption corresponds to the transition from the ground to the first excited state and is mainly described by one electron-excitation from the highest occupied molecular orbital (HOMO) to the lowest unoccupied orbital (LUMO) [36]. The energy gap for PDPO was calculated using B3LYP/6-31G(d,p) level. The bioactivity and chemical activity of the molecule depends on the eigen value of HOMO, LUMO and energy gap. LUMO as an electron acceptor represents the ability to obtain an electron; donor represents the ability to donate an electron. The frontier molecular orbitals are shown in Fig. 5. From the molecular orbital analysis the highest occupied level is 87 this locates over the C–N–C group. And the 88 is the excited frontier orbital (LUMO-π^*), this orbital located over the C_1–O_{50} and carbon atoms in phenyl ring. The energy difference between the HOMO and LUMO is about 5.288 eV. The frontier molecular orbital of PDPO (HOMO–LUMO) is shown in Fig. 5.

HOMO energy = −6.169 eV

LUMO energy = −0.881 eV

Energy gap = 5.288 eV

The smaller band gap energy increases the stability of the molecule. The charge distribution of the molecule has calculated
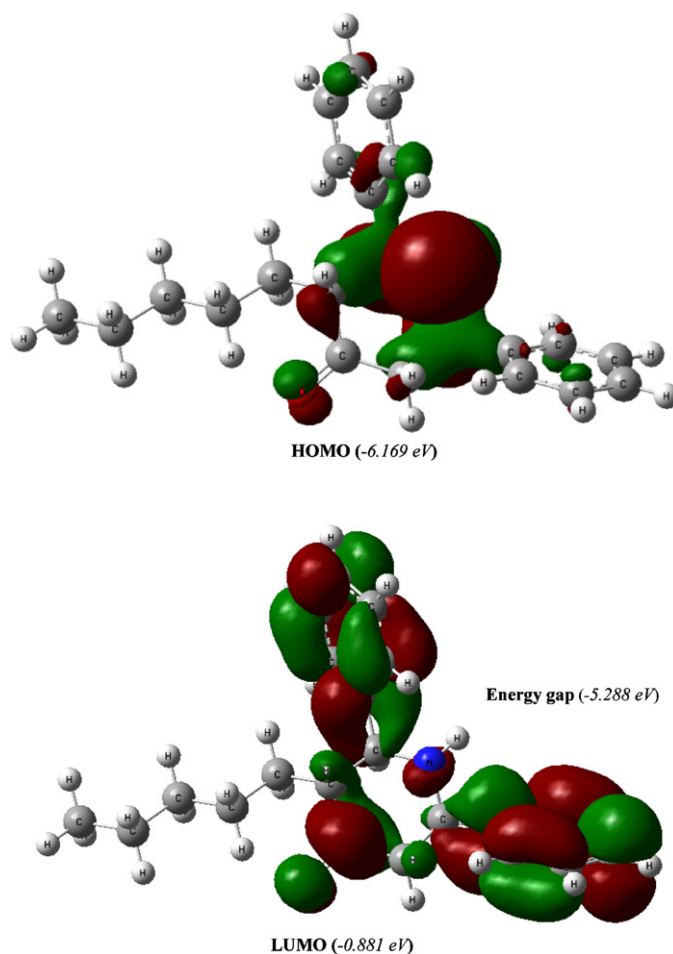

HOMO (-6.169 eV)

Energy gap (-5.288 eV)

LUMO (-0.881 eV)

Fig. 5. The frontier molecular orbital of PDPO (HOMO–LUMO).

Table 4
Atomic charge of PDPO.

Atoms	Charges (a.u.)	Atoms	Charges (a.u.)
C_1	0.402	C_{24}	0.099
C_2	−0.226	C_{25}	−0.118
C_3	−0.011	C_{26}	−0.092
C_4	0.022	C_{27}	−0.088
C_5	−0.119	C_{29}	−0.099
N_{12}	−0.515	C_{31}	−0.079
C_{13}	0.060	C_{35}	−0.178
C_{14}	−0.113	C_{36}	−0.198
C_{15}	−0.107	C_{39}	−0.173
C_{16}	−0.092	C_{42}	−0.180
C_{18}	−0.090	C_{47}	−0.318
C_{20}	−0.082	O_{50}	−0.465

using B3LYP/6-31G(d,p) level. This calculation depicts the charges of the every atom in molecule. Distribution of positive and negative charges is the cause, to increase or decrease of bond length. The atomic charges of carbon, nitrogen and oxygen are listed in Table 4, in which nitrogen atom has maximum negative charge of −0.515 and −0.465 a.u., for oxygen atom. The HOMO part is located over the N_{12}–C_3, N_{12}–C_4 orbital, is mainly due to the lone pair of electron. Some of the carbon atoms have only positive charge about C_1 (0.402), C_4 (0.022), C_{13} (0.060) and C_{24} (0.099 a.u.). This clearly explains that the LUMO exist in those areas. The Mulliken charge plot is shown in Fig. 6.
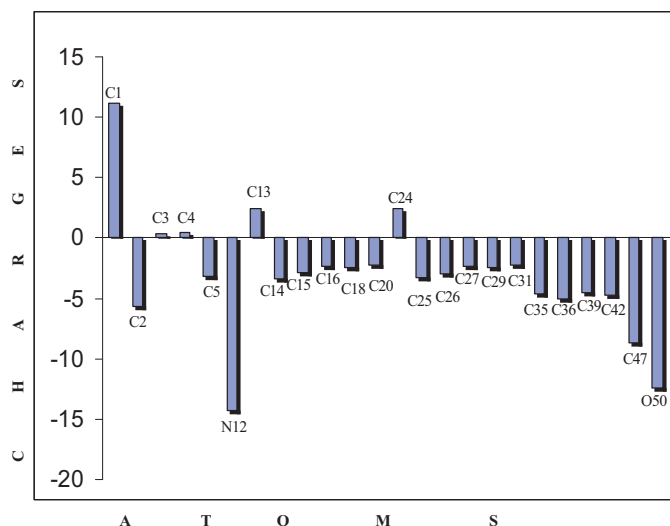
Fig. 6. Mulliken charge plot of C, N, O in PDPO.

7. Conclusion

All possible conformers are calculated by changing the torsion angle rotation with respect to bond. The calculated bond parameters are compared with reported X-ray diffraction data. All the vibrational bands which are observed in the FT-IR and FT-Raman spectra of the title compound are completely assigned for the first time with the help of TED. The donor–acceptor interaction, as obtained from NBO analysis could fairly explains the decrease of occupancies of σ bonding orbital and the increase of occupancy of π* antibonding orbitals. The bioactivity of the molecule is proposed by means of band gap (−5.288 eV) energy derived from HOMO and LUMO calculation. The atomic charges of the present molecule has been calculated and also plotted.

References

[1] R. Venketeshperumal, M. Adiraj, P. Shanmugapandian, Indian Drugs 38 (2001) 167–169.
[2] A. Numata, T. Ibuka, A. Brossi, In the Alkaloids, vol. 31, Academic Press, New York, 1987, p. 193.
[3] M.W. Edwards, J.W. Daly, C.W. Myers, J. Nat. Prod. 51 (1988) 1188–1197.
[4] C.R. Ganellin, R.G.W. Spickett, J. Med. Chem. 8 (1965) 619–625.
[5] (a) M. Srinivasan, S. Perumal, S. Selvaraj, Chem. Pharm. Bull. 54 (2006) 795;
    (b) N. Rameshkumar, A. Veena, R. Ilavarasan, M. Adiraj, P. Shanmugapandiyan, S.K. Sridhar, Biol. Pharm. Bull. 26 (2003) 188.
[6] J. Chakkaravarthy, G. Muthukumaran, K. Pandiarajan, J. Mol. Struct. 889 (2008) 297–307.
[7] P. Gayathri, J. Jayabarathi, G. Rajarajan, A. Thiruvalluvar, R.J. Butcher, Acta Cryst. 65E (2009) o3083.
[8] M.J. Frisch, G.W. Trucks, H.B. Schlegel, G.E. Scuseria, M.A. Robb, J.R. Cheeseman, J.A. Montgomery Jr., T. Vreven, K.N. Kudin, J.C. Burant, J.M. Millam, S.S. Iyengar, J. Tomasi, V. Barone, B. Mennucci, M. Cossi, G. Scalmani, N. Rega, G.A. Petersson, H. Nakatsuji, M. Hada, M. Ehara, K. Toyota, R. Fukuda, J. Hasegawa, M. Ishida, T. Nakajima, Y. Honda, O. Kitao, H. Nakai, M. Klene, X. Li, J.E. Knox, H.P. Hratchian, J.B. Cross, C. Adamo, J. Jaramillo, R. Gomperts, R.E. Stratmann, O. Yazyev, A.J. Austin, R. Cammi, C. Pomelli, J.W. Ochterski, P.Y. Ayala, K. Morokuma, G.A. Voth, P. Salvador, J.J. Dannenberg, V.G. Zakrzewski, S. Dapprich, A.D. Daniels, M.C. Strain, O. Farkas, D.K. Malick, A.D. Rabuck, K. Raghavachari, J.B. Foresman, J.V. Ortiz, Q. Cui, A.G. Baboul, S. Clifford, J. Cioslowski, B.B. Stefanov, G. Liu, A. Liashenko, P. Piskorz, I. Komaromi, R.L. Martin, D.J. Fox, T. Keith, M.A. Al-Laham, C.Y. Peng, A. Nanayakkara, M. Challacombe, P.M.W. Gill, B. Johnson, W. Chen, M.W. Wong, C. Gonzalez, J.A. Pople, Gaussian 03, Revision C.02, Gaussian Inc., Wallingford, CT, 2004.
[9] H.B. Schlegel, J. Comput. Chem. 3 (1982) 214–218.
[10] G. Rauhut, P. Pulay, J. Phys. Chem. 99 (1995) 3093.
[11] D. Michalska, Raint Program, Wroclaw University of Technology, 2003.
[12] D. Michalska, R. Wysokinski, Chem. Phys. Lett. 403 (2005) 211–217.
[13] M.T. Gulluoglu, Y. Erdogdu, S. Yurdakul, J. Mol. Struct. 834 (2007) 540–547.
[14] Y. Erdogdu, M.T. Gulluoglu, S. Yurdakul, J. Mol. Struct. 889 (2008) 361–370.
[15] Y. Erdogdu, M.T. Gulluoglu, Spectrochim. Acta 74A (2009) 162–167.
[16] W.B. Tzeng, K. Narayanan, J.L. Lin, C.C. Tung, Spectrochim. Acta 55A (1998) 153–162.
[17] N.P.G. Roeges, A Guide to the Complete Interpretation of Infrared Spectra of Organic Structures, Wiley, New York, 1994.
[18] I.H. Joe, G. Aruldhas, S.A. Kumar, P. Ramasamy, Cryst. Res. Technol. 29 (1994) 685.
[19] D. Lin-Vein, N.B. Colthup, W.G. Fateley, J.G. Grasselli, The Hand Book of Infrared and Raman Characteristic Frequencies of Organic Molecules, Academic Press, San Diego, 1991.
[20] M. Silverstein, G. Clyton Basseler, C. Morill, Spectrometric Identification of Organic Compounds, Wiley, New York, 1981.
[21] N. Sundaraganesan, S. Ilakiyamani, B.D. Joushua, Spectrochim. Acta 67A (2007) 287–297.
[22] K. Drużbicki, E. Mikuli, M.D. Ossowska-Chruściel, Vib. Spectrosc. 52 (2010) 54–62.
[23] D. Dolega, A. Migal-Mikuli, J. Chruściel, J. Mol. Struct. 933 (2009) 30–37.
[24] J.G. Mesu, T. Visser, F. Soulimani, B.M. Weckhuysen, Vib. Spectrosc. 39 (2005) 114–125.
[25] M. Barthes, G. De Nunzio, M. Ribet, Synth. Met. 76 (1996) 337–340.
[26] C.Y. Panicker, H.T. Varghese, D. Philip, H.I.S. Nogueira, K. Kastkova, Spectrochim. Acta 67 (2007) 1313–1320.
[27] Y. Erdogdu, O. Unsalan, M. Amalanathan, I.H. Joe, J. Mol. Struct. 980 (2010) 24–30.
[28] M.A. Palafox, Int. J. Quant. Chem. 77 (2000) 661–684.
[29] A.E. Reed, F. Weinhold, J. Chem. Phys. 83 (1985) 1736.
[30] A.E. Reed, R.B. Weinstock, F. Weinhold, J. Chem. Phys. 83 (1985) 735.
[31] A.E. Reed, F. Weinhold, J. Chem. Phys. 78 (1983) 4066.
[32] J.P. Foster, F. Weinhold, J. Am. Chem. Soc. 102 (1980) 7211–7218.
[33] J. Chocholousova, V. Vladimir Spirko, P. Hobza, Phys. Chem. Chem. Phys. 6 (2004) 37–41.
[34] B. Smith, Infrared Spectral Interpretation: A Systemic Approach, CRC, Washington, DC, 1999.
[35] I. Fleming, Frontier Orbitals and Organic Chemical Reactions, Wiley, London, 1976.
[36] I. Sidir, Y.G. Sidir, M. Kumalar, E. Tasal, J. Mol. Struct. 964 (2010) 134.